Journal of Harbin Engineering University
ISSN: 1006-7043
Vol 45 No. 12
December 2024

Experimental vs. FEM-Based Evaluation of Steel and GFRP Reinforced Slabs Incorporating Sustainable Materials

[1]R. Vijayalakshmi, [2]Dr. R. S. Ravichandran, [3]Dr. J. Saravanan, [4]Dr. C. Prithiviraj
[1]Research Scholar, [2]Associate Professor, [3]Professor, [4]Assistant Professor
[1,2,3]Department of Civil and Structural Engineering, [4]Department of Civil Engineering
[1,2,3]Annamalai University, Chidambaram, India.
[4]SRM Madurai College for Engineering and Technology, Sivgangai, India.

Abstract

Introduction: The increasing demand for sustainable construction materials has led to the integration of alternatives like M-sand and Alccofine into reinforced concrete slabs. This study explores the structural performance of slabs reinforced with steel and glass fiber-reinforced polymer (GFRP), aiming to enhance durability and sustainability while addressing the unique mechanical properties of both reinforcement types.

Objectives: The primary objectives of this study are to compare the structural behaviour of slabs reinforced with steel and GFRP under loading. Investigate the effects of incorporating M-sand and Alccofine on load-bearing capacity, deflection, and energy absorption. Validate finite element method (FEM) simulations against experimental data to assess predictive accuracy. Evaluate the potential of FEM for preliminary structural assessments and design optimization.

Methods: Experimental tests were conducted to evaluate load-bearing capacity, deflection, and energy absorption of slabs. A finite element model was developed in ANSYS to simulate load-deflection behaviour, stress distribution, and crack patterns. Experimental and FEM results were compared through statistical analysis, using ratios of experimental-to-FEM values and root mean square error (RMSE) to determine accuracy.

Results: Steel-reinforced slabs exhibited superior energy absorption and ductility due to steel's plastic deformation capabilities. GFRP-reinforced slabs, when paired with Alccofine and increased reinforcement ratios, showed significant performance improvement. The FEM model demonstrated an experimental-to-FEM load ratio of 1.14–1.27 and a deflection ratio of 1.09–1.36, indicating reasonable predictive accuracy despite slight underestimations, particularly in post-cracking responses.

Conclusions: This study highlights the effectiveness of FEM in structural analysis, particularly for preliminary assessments. While steel reinforcement offers superior ductility, GFRP reinforcement combined with sustainable materials like M-sand and Alccofine enhances performance, making it a viable alternative for specific structural applications. The findings provide valuable insights for optimizing composite slab designs, promoting sustainability and efficiency in construction practices.

Keywords: Sustainable Materials; GFRP Reinforcement; Steel Reinforcement; Finite Element Method (FEM); Concrete Structural Performance

1. Introduction

As the construction industry seeks sustainable alternatives to conventional materials, incorporating eco-friendly materials like glass fiber reinforced polymer (GFRP), Alccofine, and manufactured sand (M-Sand) in concrete structures has gained attention. This study, investigates the structural performance of concrete slabs reinforced with GFRP and steel bars, using Alccofine and M-Sand in the mix. Both experimental and finite element method (FEM) analyses were conducted to assess the load-bearing capacities, deflection behaviour, and suitability of these materials in reinforced concrete slabs.

GFRP is increasingly recognized as a viable alternative to steel reinforcement, particularly in structures exposed to corrosive environments. Its non-corrosive nature and high strength-to-weight ratio make it ideal for marine and coastal applications, where durability is crucial [1]. Unlike steel, GFRP does not degrade due to moisture or chemicals, enhancing the longevity of concrete structures in harsh environments [2]. Steel remains the standard for reinforcement due to its high tensile strength and ductility, yet it is vulnerable to corrosion, resulting in high maintenance costs and reduced structure lifespan [3].

Alccofine, a micro-fine slag-based material, improves concrete's compressive strength, workability, and durability [4], [5]. It makes concrete mixes denser, reducing permeability and enhancing resistance to chemical attacks, essential for high-performance applications [6]. M-Sand, an engineered alternative to natural sand, provides consistent particle size and fewer impurities, enhancing bonding and reducing shrinkage in concrete [7]. The use of GFRP, steel, Alccofine, and M-Sand not only supports sustainable construction but also optimizes structural performance. Steel reinforcement, while strong and ductile, is susceptible to environmental degradation. GFRP, in contrast, is lightweight, corrosion-resistant, and suitable for structures in aggressive environments. While GFRP's lower ductility limits its applications, it remains beneficial in reducing maintenance costs for structures like bridges, marine infrastructure, and other exposed elements. Alccofine enhances durability and density, while M-Sand, as a consistent-quality aggregate, is particularly advantageous given natural sand scarcity and environmental concerns.

Prior studies on GFRP reinforcement highlight its advantages in non-corrosive, lightweight reinforcement applications, though it lacks steel's ductility. Research indicates that GFRP is suitable for situations where corrosion prevention is crucial, particularly in coastal and industrial environments [8], [9]. However, limited studies have focused on sustainable concrete mixes containing Alccofine and M-Sand in slab applications, emphasizing the novelty of this investigation. Alccofine, known for enhancing strength and durability, creates a denser concrete matrix, reducing permeability and improving chemical resistance. This is valuable in infrastructure where long-term durability is essential. The consistent particle size of M-Sand improves bonding and workability, resulting in stronger, more durable concrete with less shrinkage compared to natural sand, and provides a sustainable alternative amid dwindling sand resources.

FEM analysis is increasingly important in structural engineering, enabling detailed simulation of stress, deflection, and failure patterns under various load conditions [10]. In this study, FEM simulations predict load-deflection behaviour and cracking patterns of slabs with GFRP and steel reinforcement, complementing experimental results and providing a deeper understanding of material performance. By simulating different configurations, FEM aids in optimizing slab designs for improved sustainability and performance.

1.1 Objectives and Significance of the Study

This research investigates the performance of concrete slabs reinforced with steel and GFRP bars, incorporating sustainable materials such as Alccofine and M-Sand. The primary goal is to assess whether increasing the GFRP reinforcement ratio can enhance slab performance to a level comparable to steel reinforcement. In previous studies, both steel and GFRP were applied with the same reinforcement ratio of 0.4, and steel exhibited superior strength and ductility under loading [11]. GFRP, although advantageous for corrosion resistance, exhibited limitations in load-bearing capacity and deflection control when matched with steel at the same reinforcement ratio.

To address this disparity, this study increases the reinforcement ratio to 0.6 specifically for GFRP-reinforced slabs, while keeping steel reinforcement at 0.4. The objective is to evaluate whether the increased GFRP ratio compensates for its lower mechanical properties, providing a similar or improved structural performance compared to the steel-reinforced slabs at a lower ratio. The results will reveal whether adjusting the reinforcement ratio can mitigate the inherent limitations of GFRP in structural applications. By comparing both experimental outcomes and FEM simulations, this study aims to deliver insights on the optimal reinforcement configurations for GFRP in sustainable concrete applications, contributing to the ongoing search for durable, eco-friendly construction materials that can compete with traditional steel reinforcement.

This investigation is significant as it may pave the way for wider application of GFRP in aggressive environments where steel would corrode, thus lowering maintenance costs and extending the life of infrastructure in coastal or industrial regions.

Moreover, these findings could guide the development of design codes and standards that accommodate GFRP with optimized reinforcement ratios, allowing for both environmental benefits and structural integrity in various applications.

1.2 Research Gaps and Novelty

Despite extensive research on GFRP, studies comparing GFRP and steel reinforcement in slabs, particularly with sustainable concrete materials like Alccofine and M-Sand, remain limited. Moreover, few studies provide a side-by-side comparison of experimental data with FEM simulations to validate the structural behaviour of these materials under similar conditions [12]. This research addresses these gaps by exploring the performance of GFRP and steel-reinforced slabs and validating FEM simulations with experimental data, contributing to the literature on sustainable construction practices.

2. Experimental Investigation

2.1 Materials

The study utilized OPC 53 grade cement, Alccofine, river sand, M-sand, steel reinforcement, and GFRP reinforcement, each conforming to relevant standards (OPC: IS 12269 [13], Alccofine: ASTM C989 [14], aggregates: IS 383 (2016) [15], steel: IS 1786 (2008) [16], and GFRP: ASTM D7957 [17]). Four concrete mixes were designed, incorporating both conventional and Alccofine-based formulations, each with a blend of river sand and M-sand for optimized aggregate distribution. Material properties and mix proportions are detailed in Tables 1 to 4.

.

Table 1 Chemical Properties of Binders

Component	CaO	SiO_2	Fe_2O_3	Al_2O_3	SO_3	MgO	K_2O	Na_2O	TiO_2	Loss of ignition
Cement	66.67	18.91	4.94	4.51	2.5	0.87	0.43	0.12	-	1.05
Alccofine	32.2	35.3	1.2	21.4	0.13	6.2	-	-	-	-

Table 2 Physical Properties of Binders and Aggregates

Description	Size	Specific gravity	Water absorption (%)	Fineness Modulus	Silt content (%)	Specific surface area
Cement	90µ	3.15	–	–	–	225m²/kg
Alccofine	4 to 6µ	2.86	–	–	–	1200m²/kg
River Sand	< 4.75mm	2.56	1.2	2.85	2.2	
M-Sand	< 4.75mm	2.65	3.07	2.9	4.8	–
Coarse Aggregate	20mm	2.7	0.5	7.1	1	–

Table 3 Properties of Reinforcements

Rebar	Tensile strength (MPa)	Yield strength (MPa)	Elastic Modulus (GPa)	Poisson Ratio
Sand Coated GFRP	290	-	62.3	0.22
Steel Fe 500	640	500	200	0.3

Table 4 Mix Proportions and Mechanical Properties

Description	CRS	CMS	ARS	AMS
Cement kg/m³	348.32	348.32	296.07	296.07
Alccofine kg/m³	-	-	52.24	52.24
River Sand kg/m³	727.15	-	727.15	-

M-Sand kg/m³	-	759.34	-	759.34
Coarse aggregate kg/m³	1204.48	1204.48	1204.48	1204.48
Water kg/m³	191.58	191.58	191.58	191.58
W/B ratio	0.55	0.55	0.55	0.55
Compressive Strength MPa	24.03	26.34	31.97	37.02
Flexural Strength MPa	3.31	3.49	3.71	3.96
Young's Modulus GPa	23.72	25.84	31.56	36.83

2.2 Specimen Preparation and Experimental Procedure

Twelve one-way reinforced concrete slabs were tested, grouped by reinforcement type and binder content as outlined in Table 5. Slabs are categorized into six groups, Groups 1 and 2 used conventional concrete with steel or GFRP reinforcement, while Groups 3 and 4 used Alccofine-based concrete with similar reinforcement. Groups 5 and 6 had increased GFRP ratios, using conventional and Alccofine-based concrete, respectively. Each group contained two slabs with either river sand or M-sand. The slabs, measuring 2000 mm × 600 mm × 125 mm, were reinforced with 12 mm bars at 280 mm c/c, for increased reinforcement ratio 186 mm c/c as primary reinforcement and 8 mm bars at 300 mm c/c as distribution reinforcement, with a 20 mm concrete cover. Cast with mix proportions from Table 4, slabs were cured for 28 days, cleaned, whitewashed, and prepared for testing on a 50-tonne load frame with roller and hinge supports. Two-point loading was applied via spreader beams, with incremental loads of 1 kN applied by hydraulic jacks up to failure. Deflections were recorded using dial gauges, strain gauges, and demec gauges positioned at key locations. Crack widths were measured at ultimate load using a microscope. The experimental setup is shown in Figure 1.

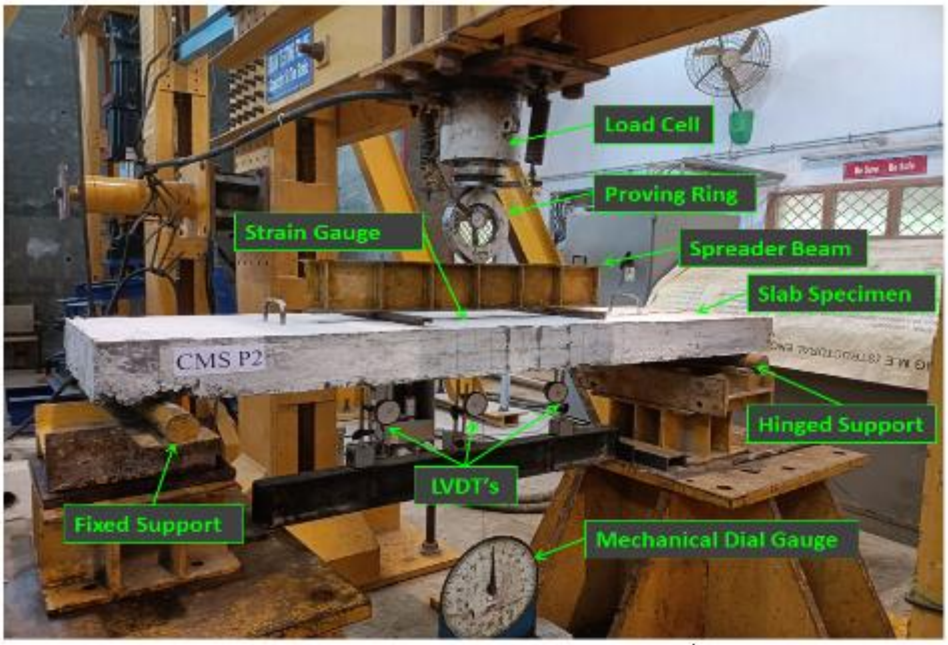

Figure 1 Experimental Test Setup

Table 5 Specimen details

Specimen Group	Slab ID	Longitudinal bar		ρ %	ρ/ρb	Predicted mode of failure
		Steel	GFRP			
Group I	CRS-S	3#12mm	-	0.4	0.022	Yield
	CMS-S	3#12mm	-	0.4	0.024	Yield

Group II	CRS-G	-	3#12mm	0.4	0.373	Rupture of Rebar
	CMS-G	-	3#12mm	0.4	0.35	Rupture of Rebar
Group III	ARS-S	3#12mm	-	0.4	0.029	Yield
	AMS-S	3#12mm	-	0.4	0.034	Yield
Group IV	ARS-G	-	3#12mm	0.4	0.299	Rupture of Rebar
	AMS-G	-	3#12mm	0.4	0.271	Rupture of Rebar
Group V	CRS-G1	-	4#12mm	0.6	0.497	Rupture of Rebar
	CMS-G1	-	4#12mm	0.6	0.462	Rupture of Rebar
Group VI	ARS-G1	-	4#12mm	0.6	0.4	Rupture of Rebar
	AMS-G1	-	4#12mm	0.6	0.361	Rupture of Rebar

The naming of specimens with the combinations of cement (C) and Alccofine (A) binders, river sand (R) and manufactured sand (M), steel (S) and GFRP (G) reinforcements. Notably, steel-reinforced slabs (CRS, CMS, ARS, AMS) were evaluated alongside GFRP-reinforced slabs (CRG, CMG, ARG, AMG) to compare the effects of traditional versus fiber-reinforced polymer reinforcement. Additionally, GFRP-reinforced slabs with an increased reinforcement ratio (CRS G1, CMS G1, ARS G1, AMS G1) were included to explore the impact of reinforcement quantity on structural performance, with the reinforcement increased only for GFRP slabs due to steel's inherently higher load-carrying capacity at the same reinforcement ratio.

3. Result and Discussion

The test outcomes and observed failure patterns for the slabs examined in this study are detailed in Table 6.

Table 6 Experimental test results

Specimen Group	**Slab ID**	**Load (kN)**		**Deflection (mm)**		**No. of crack**	**Crack width (mm)**	**Observed mode of Failure**	**Energy Absorption (kN.mm)**
		First Crack	**Ultimate**	**First Crack**	**Ultimate**				
Group I	CRS-S	13.44	58.43	1.08	48.32	15	0.34	Yield	1411.65
	CMS-S	14.77	59.07	1.1	49.08	14	0.34	Yield	1450.65
Group II	CRS-G	12.3	50.02	0.82	38.68	4	3.28	FRP rupture	967.96
	CMS-G	12.5	50.38	0.85	41.21	3	2.53	FRP rupture	1038.32
Group III	ARS-S	14.26	59.4	1.12	50.64	15	0.29	Yield	1504.51
	AMS-S	15.17	60.68	1.23	49.94	17	0.31	Yield	1515.6
Group IV	ARS-G	12.52	51.09	0.86	39.03	3	2.56	FRP rupture	996.88
	AMS-G	12.53	51.79	0.91	39.47	5	2.52	FRP rupture	1022.67
Group V	CRS-G1	13.03	59.31	1.35	42.22	7	2.87	FRP rupture	1251.15
	CMS-G1	13.18	60.18	1.42	43.45	6	2.81	FRP rupture	1308.31
Group VI	ARS-G1	13.34	61.27	1.46	42.36	6	2.89	FRP rupture	1298.73
	AMS-G1	13.51	62.45	1.45	44.25	7	2.86	FRP rupture	1382.36

3.1 Load deflection

The experimental load-deflection curves are illustrated in the Figure 2. Steel-reinforced slabs using conventional cement and river sand (CRS-S and CMS-S) provided baseline results, with ultimate loads of 58.43 kN and 59.07 kN and deflections of 48.32 mm and 49.08 mm. When Alccofine and M-sand were substituted (ARS-S and AMS-S), both load capacity and deflection improved slightly, reaching ultimate loads of 59.4 kN and 60.68 kN, and deflections of 50.64 mm and 49.94 mm. This improvement is attributed to Alccofine's pozzolanic effect and M-sand's angular particles enhancing matrix strength and interlocking. For GFRP-reinforced slabs, Alccofine and M-sand (ARS-G and AMS-G) also showed a positive effect, with ultimate loads increasing from 50.02 kN and 50.38 kN in conventional slabs (CRS-G and CMS-G) to 51.09 kN and 51.79 kN, although performance was still lower than steel-reinforced slabs. Increasing the GFRP reinforcement ratio further enhanced load and deflection, with CRS-G1, CMS-G1, ARS-G1, and AMS-G1 showing up to 19.54% and 5.42% increases in load and deflection, respectively, demonstrating improved load distribution and crack resistance. Overall, steel reinforcement remained superior in load-bearing, but Alccofine, M-sand, and increased GFRP reinforcement present sustainable, performance-boosting alternatives.

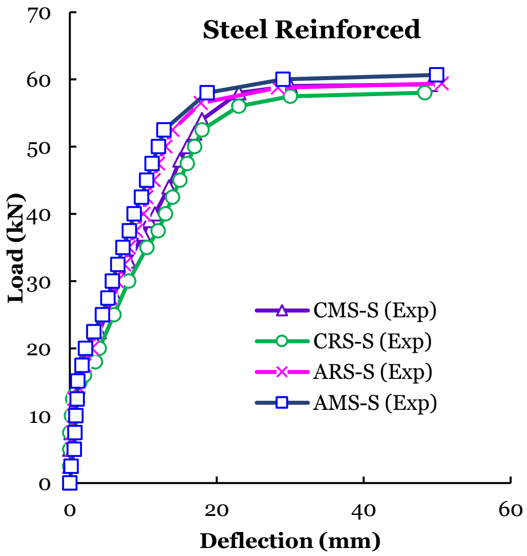

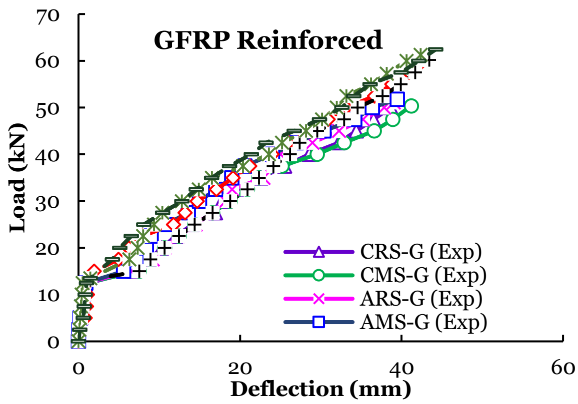

Figure 2 Experimental load-deflection curves

3.2 Cracking behaviour and failure mode

Figure 3 illustrates the deflected profile of the slabs. The experimental study revealed distinct differences in cracking behaviour and failure modes between conventional steel-reinforced slabs and those with GFRP reinforcement and substitutes like Alccofine and M-sand. Steel-reinforced slabs (CRS-S, CMS-S, ARS-S, AMS-S) had more cracks (14-17) with narrower widths (0.29-0.34 mm), indicating a ductile nature that distributes stress effectively. Alccofine's addition slightly reduced crack widths, strengthening the matrix. In contrast, GFRP-reinforced slabs (CRS-G, CMS-G, ARS-G, AMS-G, CRS-G1, CMS-G1, ARS-G1, AMS-G1) exhibited fewer (3-7) but wider cracks (2.52-3.28 mm), reflecting GFRP's brittle failure mode and limited stress distribution capacity. Steel-reinforced slabs showed ductile failure, allowing warning before collapse, while GFRP slabs experienced sudden FRP rupture, even with increased reinforcement (G1). Comparatively, steel reinforcement provided better crack control and ductility, with Alccofine and M-sand enhancing matrix strength. GFRP's brittleness limits its effectiveness in ductility, though it remains suitable for applications prioritizing corrosion resistance and lightweight properties. Additional design considerations or hybrid reinforcement may be needed for GFRP to achieve ductility akin to steel-reinforced slabs.

Figure 3 Deflected Profile of Slab Specimens

3.3 Energy absorption

In Group I, steel-reinforced cement slabs (CRS-S and CMS-S) had high energy absorption values of 1411.65 kN.mm and 1450.65 kN.mm, with CMS-S showing a 2.76% increase due to M-sand's improved bonding effect. Group II's GFRP-reinforced slabs (CRS-G and CMS-G) had lower values of 967.96 kN.mm and 1038.32 kN.mm, a 31-28% decrease from Group I, due to GFRP's brittle nature. CMS-G, however, benefited from M-sand, with a 7.27% increase over CRS-G. Group III's steel-reinforced Alccofine slabs (ARS-S and AMS-S) had the highest energy absorption (1504.51 kN.mm and 1515.6 kN.mm), showing Alccofine's benefit in strengthening the matrix. In Group IV, GFRP-reinforced Alccofine slabs (ARS-G and AMS-G) improved slightly in energy absorption over Group II, while Group V's increased GFRP ratio (CRS-G1 and CMS-G1) raised energy absorption by 29-26% over Group II. Group VI combined Alccofine with higher GFRP reinforcement, showing 30-35% gains, though still below steel-reinforced slabs. Overall, steel-reinforced slabs had superior energy absorption due to ductility, while Alccofine and higher GFRP reinforcement ratio enhanced energy absorption in GFRP slabs, though brittleness remained a limiting factor. These findings underscore steel's superior performance in energy dissipation and Alccofine's positive impact.

4. Numerical Investigation

The numerical investigation was conducted using ANSYS software to simulate the behaviour of one-way reinforced concrete slabs under various reinforcement and binder configurations. ANSYS, known for its robust finite element analysis capabilities, enabled detailed examination of load-deflection behaviour, stress distribution, and crack propagation. SOLID65 elements were used to model concrete, capturing nonlinear behaviours like cracking and crushing, while LINK180 elements represented steel and GFRP reinforcements. A refined mesh was applied, optimized for accuracy and computational efficiency. Material properties, including compressive and tensile strengths and modulus of elasticity, were set based on experimental values for both conventional and Alccofine-based concretes, with distinct properties assigned to steel and GFRP reinforcements. Boundary conditions, supports, and load points mirrored the experimental setup, allowing for reliable comparisons and in-depth analysis of slab performance, load capacity, and failure modes. The modelling, meshing and boundary conditions are shown in Figure 4.

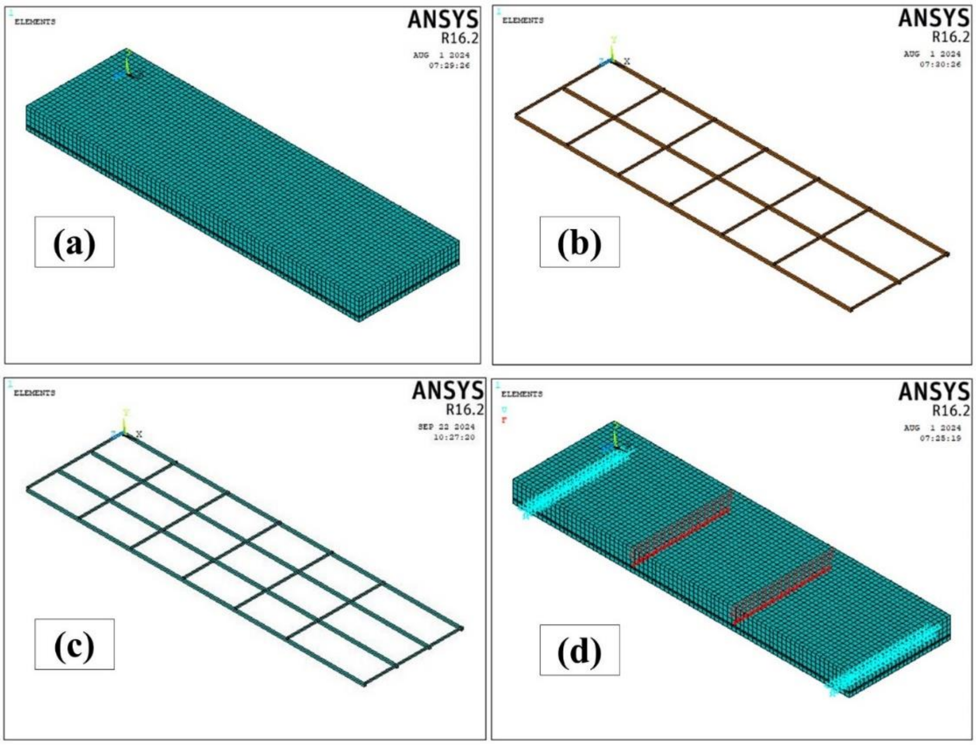

Figure 4 FEM Model a) Modelling and Meshing, b) & c) Reinforcement gauge for the ratio 0.4 and 0.6, d) Load applied & support condition assigned

4.1 Load-Deflection Curves

Table 7 displays the comparison of load-deflection results of experimental and numerical. The load-deflection curves obtained from the FEM simulations were compared with those from the experimental tests for each slab type (Figure 5). The FEM-predicted curves generally followed a similar trend to the experimental curves, showing an initial linear phase followed by a nonlinear increase in deflection as the load approached the ultimate capacity. However, discrepancies were observed, with the FEM predictions underestimating both the load capacity and deflection at the ultimate load stage across all slab configurations. For example, in conventional steel-reinforced slabs (e.g., CRS-S and CMS-S), the FEM model predicted a maximum load that was approximately 76–80% of the experimental ultimate load. Similarly, deflection values from FEM were consistently lower, with an average difference of around 20–30% at peak load. These discrepancies are likely due to the idealized assumptions in the FEM, which may not fully account for the complex interactions between reinforcement and concrete, as well as the material properties of Alccofine and M-sand used in replacement-based slabs. The load-deflection discrepancies highlight the need for more accurate modelling of material nonlinearities in FEM. For instance, incorporating material damage models or refining the meshing techniques around reinforced areas could potentially improve the alignment of FEM predictions with experimental observations. The deflected profiles of FEM-modelled slab specimens are illustrated in Figure 6.

Table 7 Comparison of Experimental and FEM results

Specimen Group	Slab ID	ρ/ρb	Experimental		FEM		Exp/FEM (ratio)	
			Load (kN)	Deflection (mm)	Load (kN)	Deflection (mm)	Load (kN)	Deflection (mm)
Group I	CRS-S	0.022	58.43	48.32	47.00	36.72	1.24	1.32
	CMS-S	0.024	59.07	49.08	47.50	39.54	1.24	1.24
Group II	CRS-G	0.373	50.02	38.68	42.50	31.55	1.18	1.23

	CMS-G	0.350	50.38	41.21	42.75	32.17	1.18	1.28
Group III	ARS-S	0.029	59.40	50.64	47.25	37.12	1.26	1.36
	AMS-S	0.034	60.68	49.94	47.75	37.58	1.27	1.33
Group IV	ARS-G	0.299	51.09	39.03	44.75	33.14	1.14	1.18
	AMS-G	0.271	51.79	39.47	44.75	34.72	1.16	1.14
Group V	CRS-G1	0.497	59.31	42.22	48.50	38.23	1.22	1.10
	CMS-G1	0.462	60.18	43.45	48.50	38.81	1.24	1.12
Group VI	ARS-G1	0.400	61.27	42.36	50.50	38.94	1.21	1.09
	AMS-G1	0.361	62.45	44.25	51.22	39.75	1.22	1.11

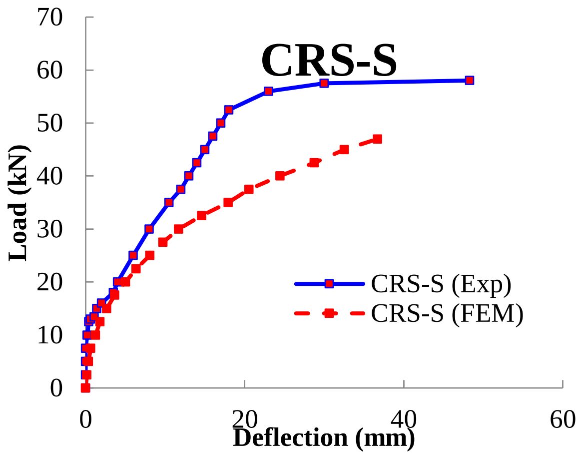

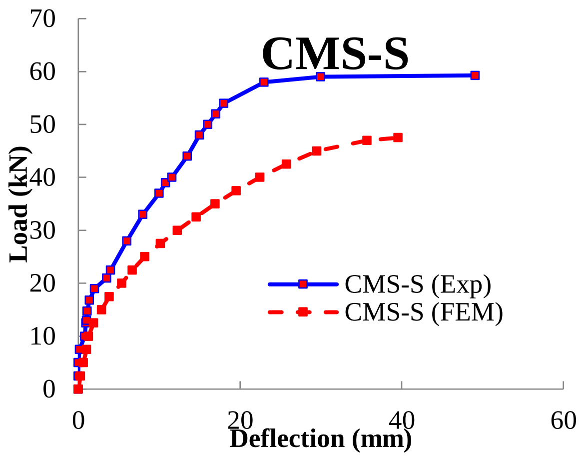

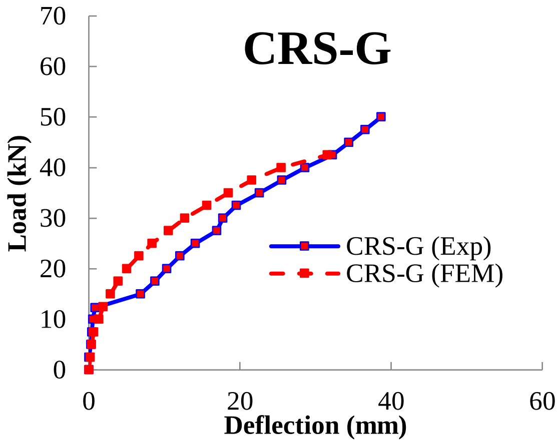

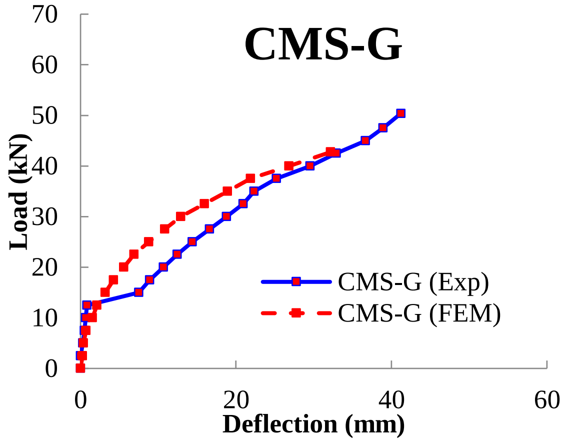

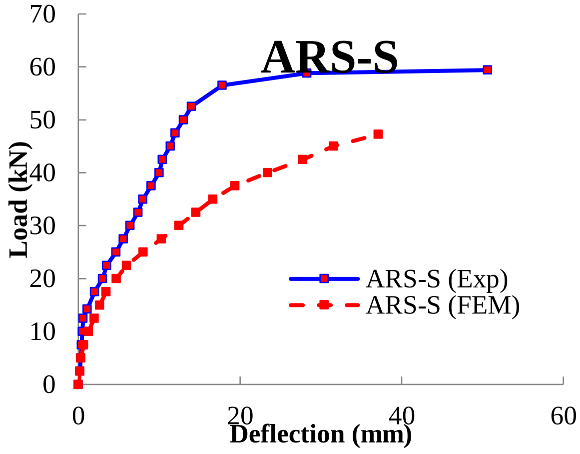

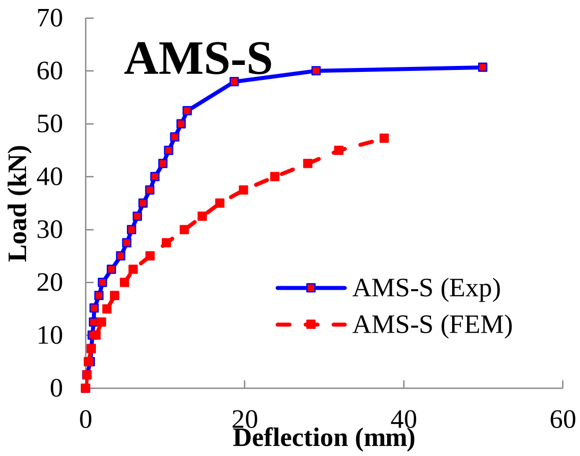
AMS-S
AMS-S (Exp)
AMS-S (FEM)
Load (kN)
Deflection (mm)

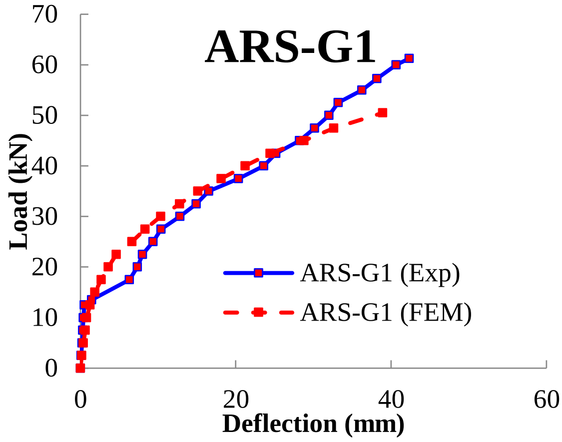
ARS-G1
ARS-G1 (Exp)
ARS-G1 (FEM)
Load (kN)
Deflection (mm)

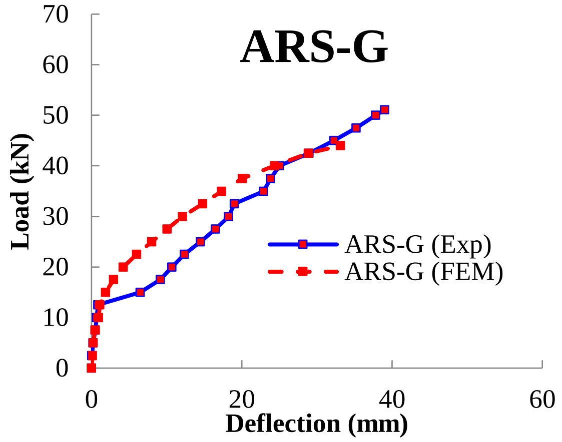
ARS-G
ARS-G (Exp)
ARS-G (FEM)
Load (kN)
Deflection (mm)

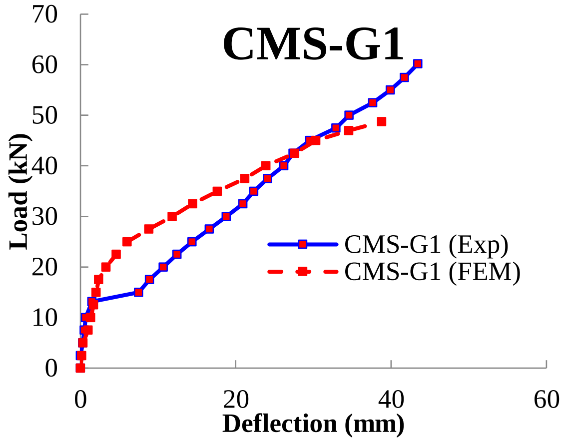
CMS-G1
CMS-G1 (Exp)
CMS-G1 (FEM)
Load (kN)
Deflection (mm)

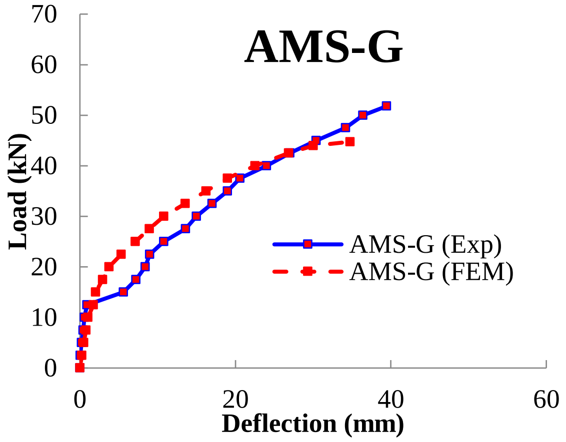
AMS-G
AMS-G (Exp)
AMS-G (FEM)
Load (kN)
Deflection (mm)

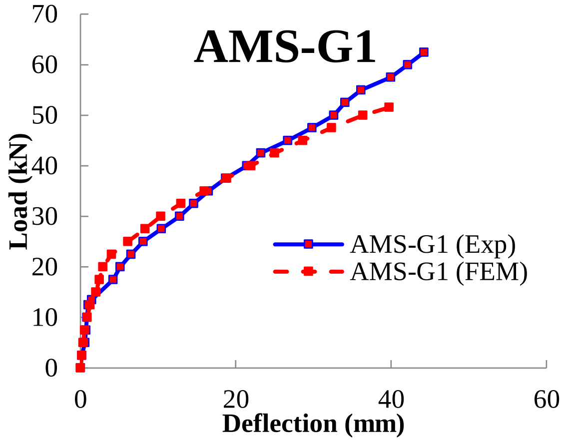
AMS-G1
AMS-G1 (Exp)
AMS-G1 (FEM)
Load (kN)
Deflection (mm)

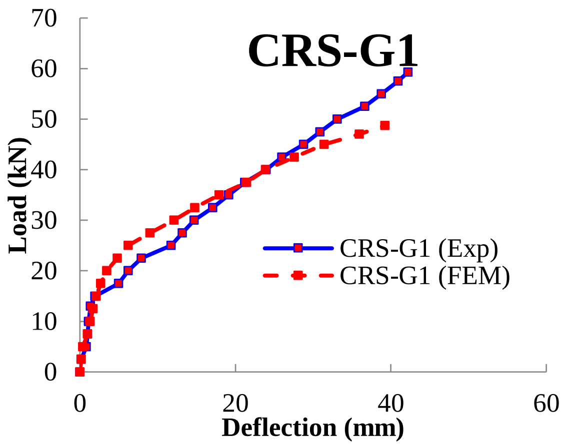
CRS-G1
CRS-G1 (Exp)
CRS-G1 (FEM)
Load (kN)
Deflection (mm)

Figure 5 Comparison of Load deflection curves for experimental and numerical

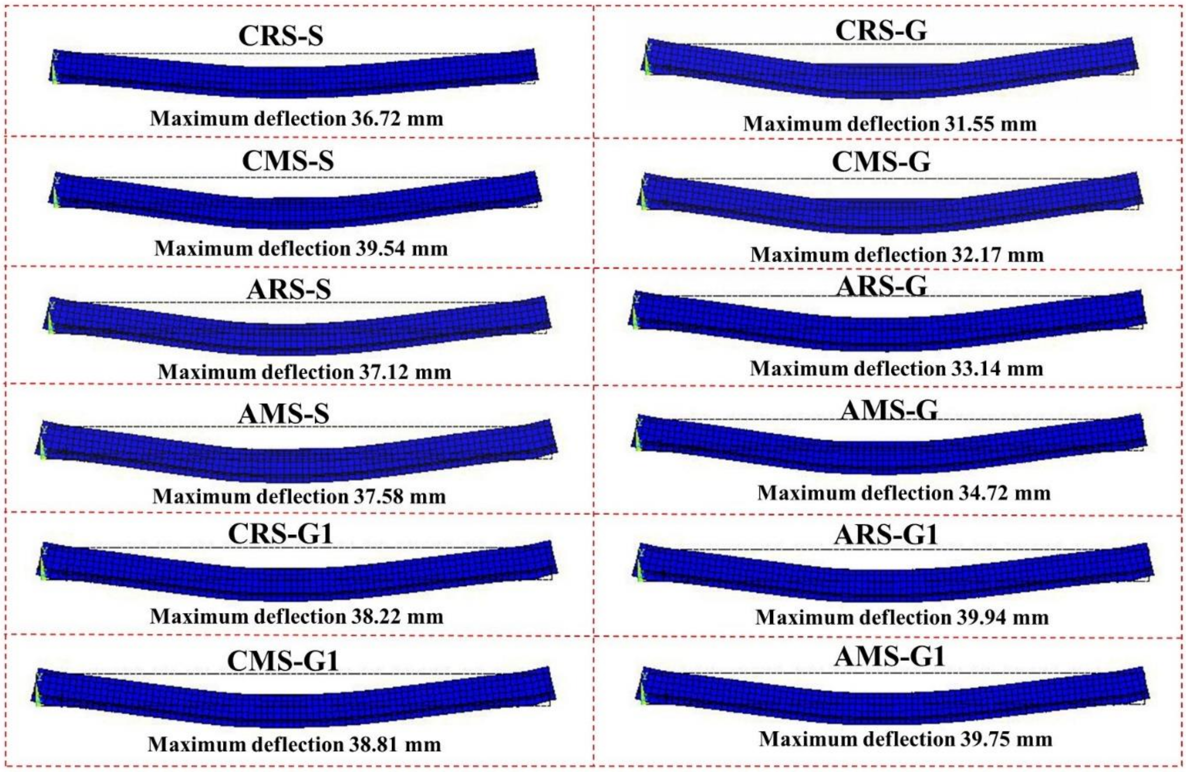

Figure 6 Deflected profiles of FEM slabs

4.2 Stress Distribution and Crack Patterns

The FEM analysis provided insights into the stress distribution across the slabs under loading and it is illustrated in Figure 7. In conventional steel-reinforced slabs, the FEM predicted high-stress concentrations near the supports and at mid-span, which aligns with the experimental observations where cracks were first observed in these regions. However, in GFRP-reinforced slabs, the stress distribution appeared more uniform, with fewer pronounced stress concentrations, reflecting the brittle nature of GFRP in tension. The FEM-predicted crack patterns (Figure 8) were compared with the observed crack propagation in the experimental tests. In conventional slabs, FEM showed ductile failure modes with widespread cracking, which was consistent with the experimental crack patterns. However, in replacement slabs with GFRP, the FEM model predicted sudden failure due to FRP rupture at lower deflection values. The experimental results also showed FRP rupture but with slightly higher crack widths and fewer cracks overall. This difference can be attributed to limitations in the FEM's ability to simulate the post-cracking behaviour of composite materials like GFRP-reinforced concrete. Overall, the FEM provided a reasonable prediction of stress distribution and initial crack propagation but tended to underestimate the crack width and extent of cracking in GFRP-reinforced slabs. These findings suggest that while FEM can accurately predict initial crack formation, enhancements in the cracking model are necessary to fully capture the post-cracking behaviour and failure modes of composite slabs.

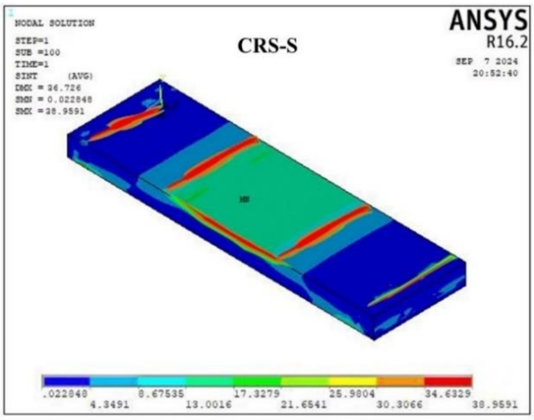

Vol 45 No. 12
December 2024

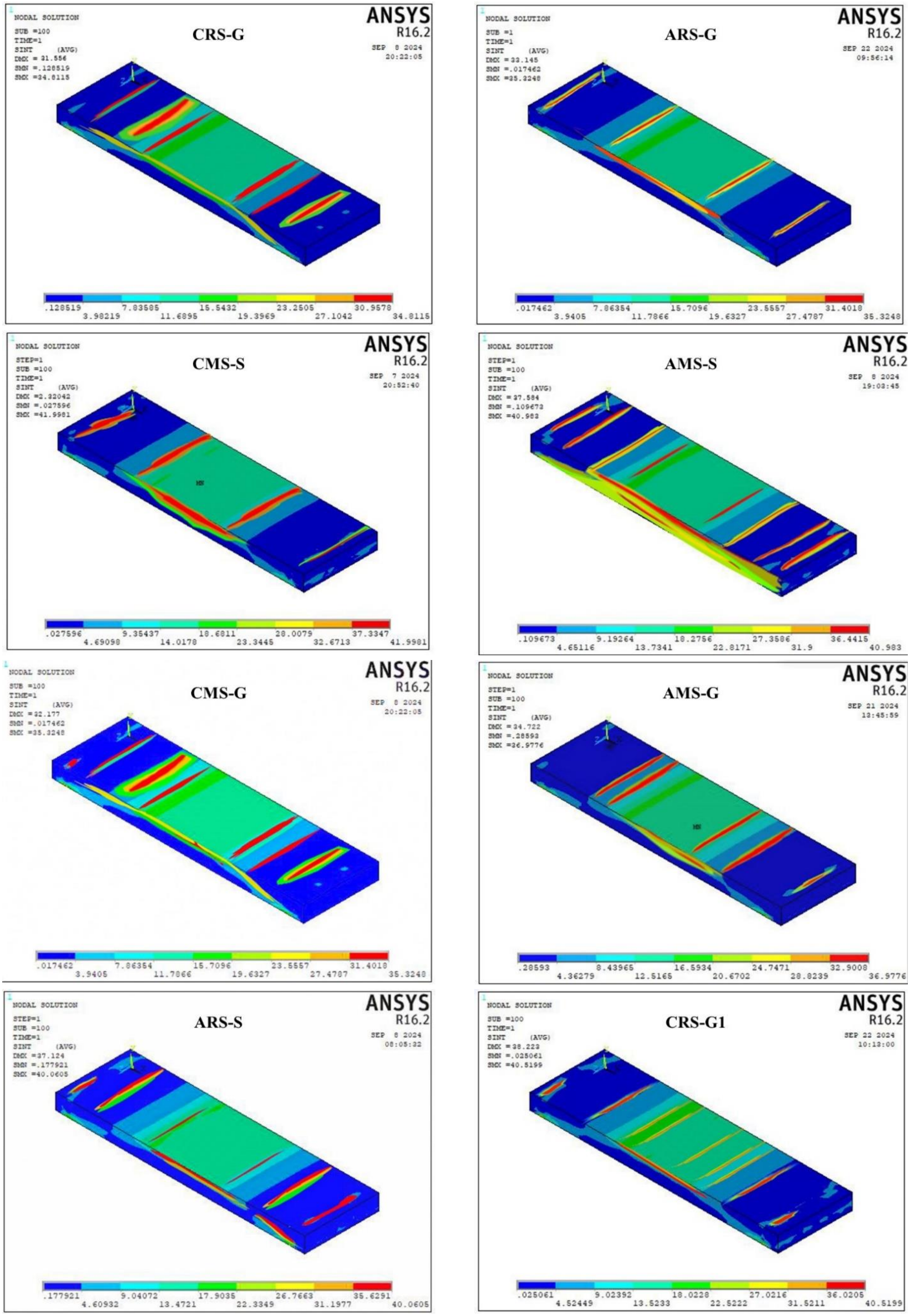

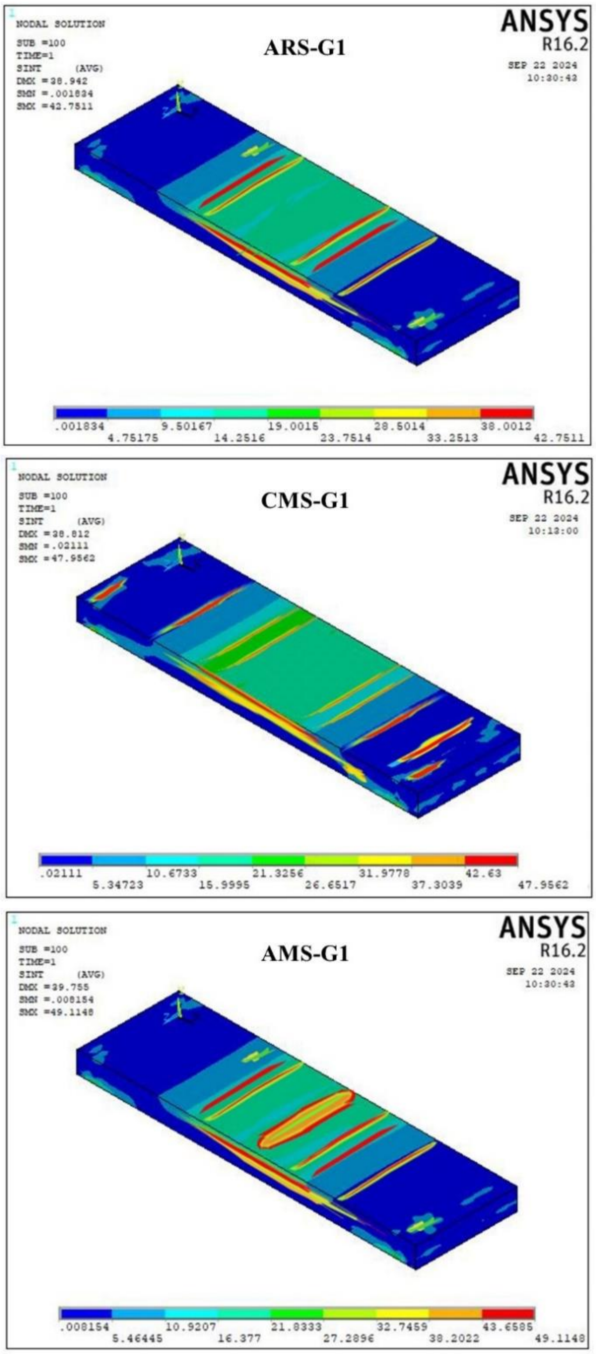

Figure 7 FEM modelled Stress distribution of slabs

4.3. Validation of FEM Results

To statistically validate the FEM results, the experimental and FEM-predicted data were compared in terms of load and deflection at key points (e.g., first crack, ultimate load). The experimental-to-FEM load ratios ranged from 1.14 to 1.27, and deflection ratios varied from 1.09 to 1.36, indicating a consistent underestimation of both load and deflection in the FEM predictions. The root mean square error (RMSE) and coefficient of determination (R^2) were calculated to assess the accuracy of the FEM model. The R^2 value of 0.89 indicates a strong, though not perfect (Figure 9), correlation between the experimental and FEM results. Additionally, the RMSE values 10.32 kN for load and 8.26 mm for deflection provide further insight into the model's performance, showing moderate discrepancies that may arise from modelling assumptions, such as idealized material properties and boundary conditions. While these RMSE values confirm that the FEM model is reasonably accurate for preliminary assessments, they also suggest that refinement could further improve precision, especially for applications demanding higher accuracy.

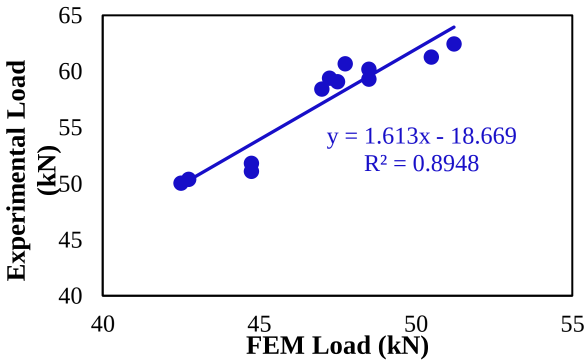

Figure 9 Correlation between Experimental and Numerical load values

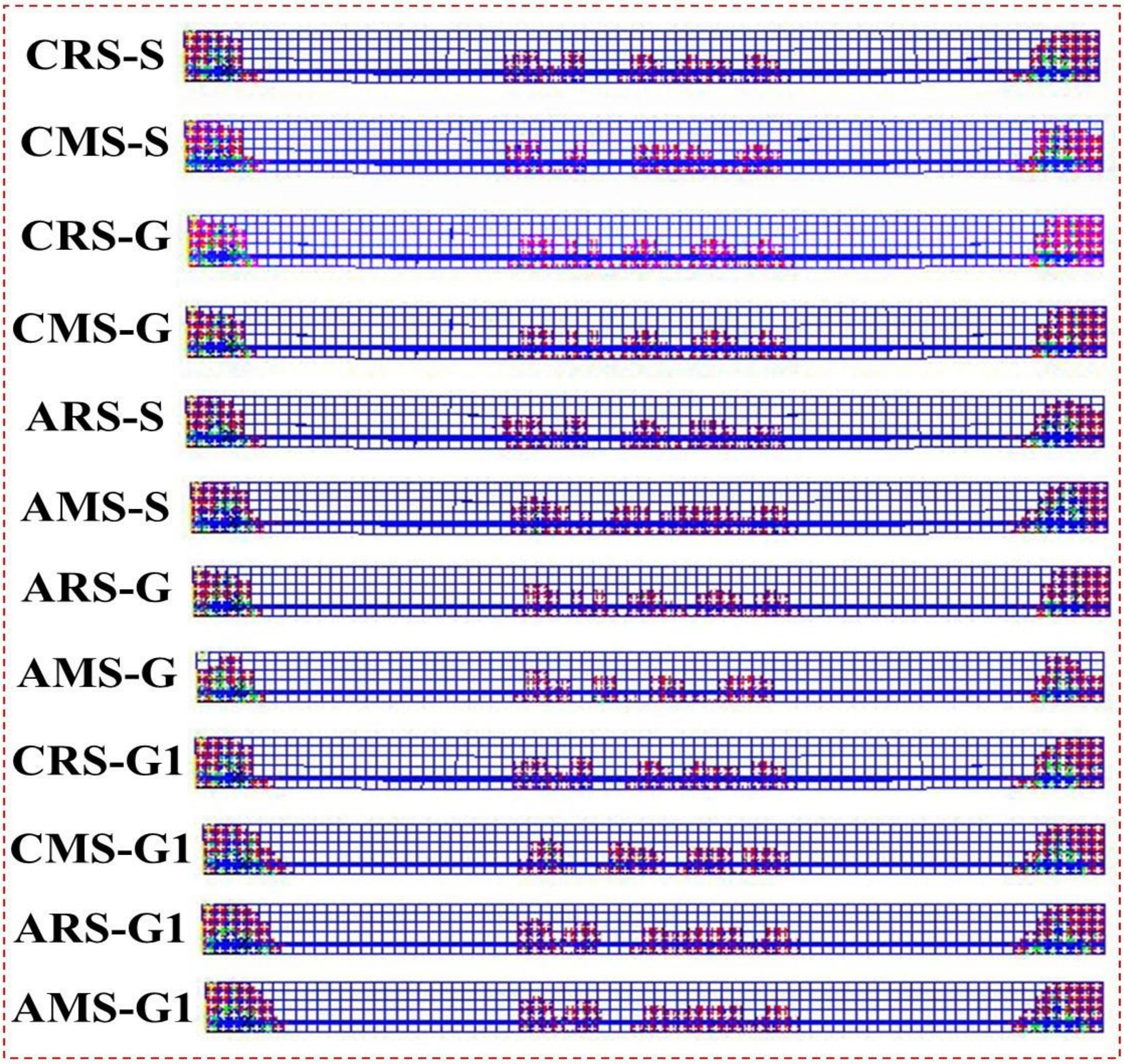

Figure 8 Crack pattern for the FEM-modelled specimens

The validation analysis demonstrates that the FEM model, while conservative, provides a relatively accurate representation of slab behaviour up to the cracking stage. However, for ultimate load and post-cracking behaviour, the FEM predictions deviate from experimental observations. These findings underscore the limitations of FEM in capturing the nonlinear, post-cracking responses of composite slabs, particularly in cases involving GFRP reinforcement and Alccofine-modified concrete.

5. Conclusion

- Steel vs. GFRP Performance: Steel-reinforced slabs demonstrated better crack control, ductility, and energy absorption than GFRP-reinforced slabs, which showed a more brittle failure mode with fewer, wider cracks.
- Impact of Sustainable Materials: Adding M-sand and Alccofine improved the performance of both steel and GFRP-reinforced slabs. Alccofine, in particular, enhanced the concrete matrix, boosting load-bearing capacity and energy dissipation in steel-reinforced slabs.
- GFRP Limitations and Improvements: GFRP-reinforced slabs, while limited in ductility, saw moderate improvements in energy absorption and crack resistance when combined with M-sand, Alccofine, and increased GFRP reinforcement.
- FEM Accuracy: FEM simulations successfully captured key experimental behaviours, including crack patterns, load-deflection responses, and

failure modes, especially in modelling GFRP's brittleness and limited energy dissipation.

- Applications and Recommendations: Steel-reinforced slabs are ideal for applications needing high energy absorption and ductility. GFRP, with sustainable materials, suits applications prioritizing lightweight and corrosion resistance. Hybrid reinforcement and advanced material research are recommended to further optimize GFRP performance.

References

[1] S. Ramanathan, V. Benzecry, P. Suraneni, and A. Nanni, "Condition assessment of concrete and glass fiber reinforced polymer (GFRP) rebar after 18 years of service life," Case Stud. Constr. Mater., vol. 14, p. e00494, 2021, doi: 10.1016/j.cscm.2021.e00494.

[2] W. Wu, X. He, W. Yang, M. S. Alam, B. Wei, and J. He, "Degradation factors and microstructure degradation characteristics of B/GFRP bars in harsh environment: A review," Constr. Build. Mater., vol. 366, no. October 2022, p. 130246, 2023, doi: 10.1016/j.conbuildmat.2022.130246.

[3] E. Mokhtari, A. Heidarpour, and F. Javidan, "Mechanical performance of high strength steel under corrosion: A review study," J. Constr. Steel Res., vol. 220, no. February, p. 108840, 2024, doi: 10.1016/j.jcsr.2024.108840.

[4] P. Chidambaram and S. Jagadeesan, "Characteristics of Self-Compacting Concrete with Different Size of Coarse Aggregates and Alccofine," Trends Sci., vol. 19, no. 5, 2022, doi: 10.48048/tis.2022.3042.

[5] C. Prithiviraj and J. Saravanan, "Influence of W/B Ratio and Chemical Admixture on Fresh and Hardened Properties of Self Compacting Concrete using Alccofine," J. Xidian Univ., vol. 14, no. 5, pp. 4906–4915, 2020, doi: 10.37896/jxu14.5/537.

[6] C. Prithiviraj, J. Saravanan, D. R. Kumar, G. Murali, N. I. Vatin, and P. Swaminathan, "Assessment of Strength and Durability Properties of Self-Compacting Concrete Comprising Alccofine," Sustain., vol. 14, no. 10, p. 5895, May 2022, doi: 10.3390/su14105895.

[7] S. Ramkumar and R. Dineshkumar, "Experimental study on impact on fineness of sand and M-sand in M20 grade of concrete," Mater. Today Proc., vol. 21, no. xxxx, pp. 36–40, 2020, doi: 10.1016/j.matpr.2019.05.356.

[8] C. Prithiviraj and J. Saravanan, "Flexural Performance of Alccofine-based Self-Compacting Concrete Reinforced with Steel and GFRP Bars," Int. Trans. J. Eng. Manag. Appl. Sci. Technol., vol. 12, no. 8, pp. 1–12, 2021, doi: 10.14456/ITJEMAST.2021.168.

[9] P. Chidambaram and S. Jagadeesan, "Analysis of GFRP-reinforced beams in enhanced SCC," Gradjevinar, vol. 76, no. 6, pp. 515–530, 2024, doi: 10.14256/JCE.3852.2023.

[10] S. T. Hasan and S. A. A. Shah, Modelling Non-Linear Response of Sic Reinforced Aluminum Alloy, vol. 1. Elsevier Ltd., 2016. doi: 10.1016/b978-0-12-803581-8.04014-5.

[11] V. Ravichandran, R. R. Srinivasan, S. Jagadeesan, and C. Prithiviraj, "Exploring the Synergy : Experimental and Theoretical Investigation of Steel and Glass Fiber Reinforced Polymer (GFRP) Reinforced Slab Incorporating Alccofine and M-Sand," Open Journnal Civ. Eng., vol. 14, pp. 334–347, 2024, doi: 10.4236/ojce.2024.143017.

[12] M. del Río Merino and J. Santa Cruz Astorqui, "Finite element simulation to design constructive elements: An application to light gypsum plaster for partitions," Constr. Build. Mater., vol. 23, no. 1, pp. 14–27, 2009, doi: 10.1016/j.conbuildmat.2007.12.009.

[13] IS:12269-2013, "Ordinary Portland Cement , 53 grade specification," Indian Stand., no. March, pp. 1–14, 2013.

[14] ASTM C989/C989M-18a, "Standard Specification for Slag Cement for Use in Concrete and Mortars," ASTM Int., pp. 1–3, 2018, doi: 10.1520/C0989.

[15] IS:383-2016, "Specification for coarse and fine aggregates from natural sources for concrete, New Delhi, India; 2016.," Indian Stand., pp. 1–24, 2016.

[16] IS:1786, "High strength deformed steel bars and wires for concrete reinforcement— specification," Indian Stand., pp. 1–12, 2008.

[17] ASTM D7957/D7957M-22, "Standard Specification for Solid Round Glass Fiber Reinforced Polymer Bars for Concrete Reinforcement," ASTM Int., pp. 1–5, 2022, doi: 10.1520/D7957.